Phase and amplitude interferometric characterization of infrared nanostructured gratings

Bruno Toulon[a], Grégory Vincent[a,b], Riad Haïdar[a], Stéphane Collin[b], Nicolas Guérineau[a], Jean-Luc Pelouard[b] and Jérôme Primot[a]

[a] ONERA, Chemin de la Hunière, F-91761 Palaiseau Cedex, France;
[b] LPN/CNRS, route de Nozay, F-91460 Marcoussis, France;

ABSTRACT

Sub-wavelength gratings allow to code complex transmittance functions that introduce both amplitude and phase variations in the propagation of a given wavefront. These micro-structures are a promising technique to miniaturize optical functions such as light polarizing, light confinement, spectral filtering... Realizations in the visible and the infrared domain have been fulfilled: for example micro-lenses, anti-reflection coatings or sinusoidal-transmittance can easily be coded. This technique is all the more advantageous in the mid-wavelength infrared (MWIR) or long-wavelength infrared (LWIR) spectral range since there are only a few materials available in this spectral range. However the characterization of these structures is problematical, since it involves phase and amplitude measurements. It is even more complicated in the far infrared domain ($8-14\,\mu$m), as will be detailed. Besides, the finite size of the gratings introduces phase steps, which is well-known to be a problematic issue. We describe here a dedicated bench to characterize sub-wavelength gratings in the LWIR spectral range. The core of the bench is a quadri-wave lateral shearing interferometer based on a diffraction grating, which allows a complete two-dimensional characterization of both phase and amplitude in a single measurement. We present here theoretical and experimental results of a characterization of such a sub-wavelength grating.

Keywords: Interferometry, nanotechnology, sub-wavelength structures, infrared

1. NANOSTRUCTURED GRATINGS

1.1 Introduction

For the last decades, nanoengineering has become a new challenge for scientists. Indeed, if we focus on the particular field of optics, engineers now require tools to miniaturize and integrate various optical functions, and the high maturity of the microelectronics allows to structure the matter at the scale of the light wavelength. They are a myriad of applications,[1] among them: realization of narrow spectral filters, coding of optical transmittances or flat lenses with planar technological processes, creating new material (called *metamaterials*) and then new optical indexes... The last point, called optical index engineering,[2] is of great interest for example in the infrared domain where the number of transparent materials is limited.

However, whereas fabrication means are numerous, the characterization process is problematical. Indeed classical techniques such as scanning electron microscopy (SEM) only yield geometrical properties of the studied structure. This is useful as quality control of deposits and their thickness or period, but not sufficient since metamaterials induce spectral or spatial resonance effects, which are highly dependant from intrinsic parameters of the processed device such as uniformity, roughness... The measurement of the optical signature of the processed device is then necessary.

Moreover, metamaterials being structured at a sub-wavelength scale, they behave, within some limitations, as homogeneous materials.[3,4] The determination of this new media properties (such as *effective* permittivity and permeability tensors) can be done by measuring optical properties such as transmission, reflection and absorption through the optical spectrum.

Contacts:
Riad Haïdar: riad.haidar@onera.fr
Jérôme Primot: jerome.primot@onera.fr

Optical Fabrication, Testing, and Metrology III, edited by Angela Duparré, Roland Geyl
Proc. of SPIE Vol. 7102, 710204 · © 2008 SPIE · CCC code: 0277-786X/08/$18 · doi: 10.1117/12.797410

1.2 Optical properties of sub-wavelength metallic gratings

In the following we are to dwell upon periodic sub-wavelength metallic structures, in which the main phenomenon is interaction between incident light and surface plasmons (surface plasmon polaritons, SPP). The structure is designed for the mid-infrared.

The structure, schematized on Fig. 1, is deposited on a gallium arsenide (GaAs) substrate which is both side coated by a quarter-wave (with a working wavelength $\lambda = 7\ \mu$m) dielectric layer (silicon nitride, Si_3N_4, for example) which acts as an anti-reflection (AR) coating. Notice that a strong absorption occurs above the wavelength $\lambda = 9\,\mu$m. The metallic grating is defined by electron-beam lithography and titanium/gold layers are then deposited thanks to electron-beam assisted evaporation. The details of the technological process are given in Ref. 5.

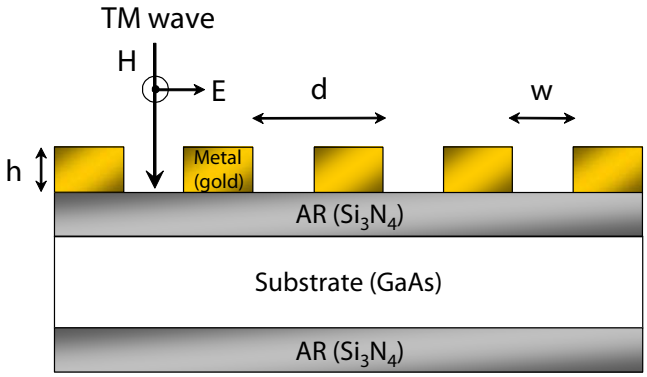

Figure 1. Definition of the geometrical parameters of the sub-wavelength gratings (d, h and w). The substrate is double-side anti-reflection (AR) coated, and the incident wave is transverse magnetic (TM) polarized, which is the polarization of the only propagative mode for narrow slits.[6]

These structures allow to code various transmittances $\tau(x) = E_{\text{out}}/E_{\text{in}} = t(x)\exp(i\phi(x))$ (where E_{in} and E_{out} are respectively the incident and the output TM polarized wave) by modifying their geometrical parameters d, h and w. Only the transmission of a TM wave is affected by the grating. This transmittance can be computed thanks to a one-mode model described in the literature.[6,7] The parameters d is chosen so as to avoid diffraction in the air or in the substrate, and h is chosen so as to strongly attenuate non-propagative modes – and both are chosen so as to stay within the validation zone of the model. The last free parameter to modify the transmittance is then the slit width w. Fig. 2 shows the complex transmittance τ as a function of the slit width. Notice that both the modulus $t(x)$ and the phase $\phi(x)$ are reported.

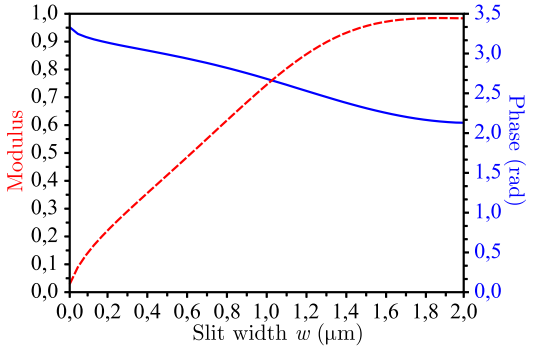

Figure 2. Modulus t (dashed red) and phase ϕ (blue) of the complex transmittance τ as a function of the grating slit w. The period is $d = 2\ \mu$m, the height is $h = 830$ nm and the working wavelength is $\lambda = 8\ \mu$m.

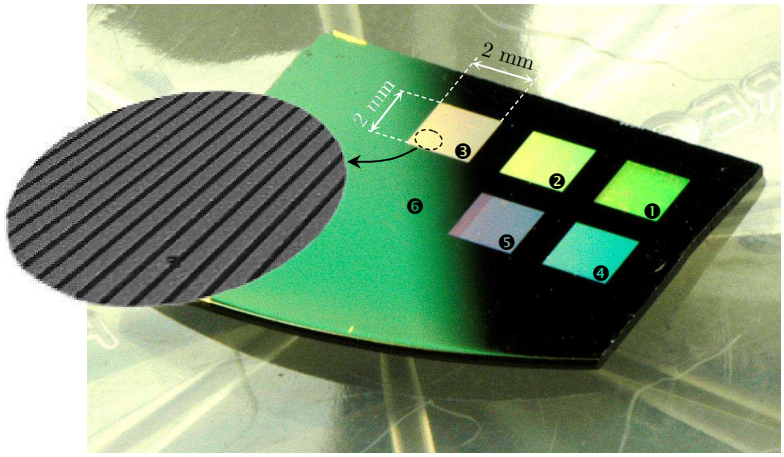

Figure 3. Illustration of the demonstrator. Each zone of transmittance τ_n is designated by a number (❶ to ❻). A scanning electron microscope zoom is presented for the grating 3.

1.3 Design and fabrication

A demonstrator has been fabricated according to the previous description. We chosen $d = 2\,\mu$m and $h = 830\,$nm. Its surface is divided in six domains (Fig. 3); each one codes a specific complex transmittance $\tau_n = t_n \cdot \exp(i\phi_n)$, where $n \in \{1 \dots 6\}$. Each transmittance area has a surface of $2 \times 2\,\text{mm}^2$ and corresponds to a given slit width w_n. The AR coating thickness is 800 nm for the grating side and 850 nm for the back side.

The grating parameters for each zone ❶ to ❻, just as the computation of the transmittance are given in Table 1.

Grating	1	2	3	4	5	6
Slits width w_n (nm)	430	780	1130	1180	1460	∞
Period d (μm)	2	2	2	2	2	$\times$
Calculated transmission $\lvert t_n\rvert^2$ (%)	17.1 %	45.3 %	77.5 %	81.2 %	94.3 %	92.9 %
Calculated phase ϕ_n (rad)	0.88	0.66	0.40	0.36	0.17	0

Table 1. Parameters of the six domains of the demonstrator. Notice that the modulus is given through the intensity transmission $|t_n|^2$ since the measure is generally done with a quadratic detector. The gold thickness is 830 nm and the working wavelength is 8 μm. The transmission assumes a transverse magnetic (TM) polarization.

1.4 Characterization: requirements and state-of-the-art

As we wrote in introduction, the optical characterization of sub-wavelength gratings is ideally spatially and spectrally resolved so as to measure all the resonant effects. Moreover a simultaneous measurement of the induced phase shift and transmission is advantageous.

Various techniques have been proposed. The spectral transmission can be evaluated by a spectrophotometer,[8] an optical spectrum analyzer[9] or a Fourier-Transform Infrared spectrometer (FTIR).[10] All these techniques meet the requirement of spectral resolution, but do not allow a spatially-resolved evaluation of the transmission.

Authors have also proposed variations on the phase delay measurement. Let's cite the use of *walk-off* or polarization interferometer:[8,11] the walk-off interferometer is made of a calcite crystal which splits the incident beam into two orthogonally polarized beams; one of them passes through the metamaterial whereas the other only passes through the glass substrate; after recombination thanks to another calcite crystal, the phase delay can be evaluated. This technique allows to measure the phase delay introduced on a polarized beam. The polarization interferometer allows to measure the phase difference between orthogonally polarized beams, which allows to qualify the anisotropy of the metamaterial. Ref. 10 proposed an indirect measurement of the phase *via*

another sample. Finally, the use of a Michelson interferometer and a 170-fs pulsed laser[12] can lead to the phase and group time delay thanks to the analysis of the fringes and enveloppe of the interferogram.

It is noteworthy that none of the proposed techniques allows a simultaneous phase and intensity measurement, nor a spatially-resolved one. Moreover the implementation can be problematical. That is why we propose in the following a characterization bench[13] based on the well-known technique of lateral shearing interferometry.

2. CHARACTERIZATION BENCH

2.1 Bench core: the quadri-wave lateral shearing interferometer

Lateral shearing interferometers (LSIs) are well-known wave-front sensors.[14] They are used in various applications from classical optical testing to atmospheric turbulence analysis or laser beam evaluation. The technique basis is to split the beam under study and to make the replicas interfere. As the wave front is analyzed by its own replica, the measure is self-sufficient and does not require a reference wave; this is a major advantage in term of implementation easiness.

There are many devices to split the incident wave front. Here we focus on diffraction-based LSIs, which means that the replicas are produced by a diffraction grating. This class of LSI offers many advantages: easy setting, compactness, achromaticity...[15] An evolution of the classical device was proposed and called multi-wave LSI,[16–18] which makes use of three or more replicas. The interferogram leads to the wave front analysis in several directions. This allows a robust determination of a surface. Whatever the replication device, the interferogram is sensitive to the difference Δ_ϕ between the phases of a couple of replicas, for example:

$$\Delta_\phi(x,y) = \phi\left(x + \frac{s}{2}, y\right) - \phi\left(x - \frac{s}{2}, y\right),$$

where s is the lateral shearing distance along the x-direction. This expression can be approximated by the derivative of the phase function $\frac{\partial\phi(x,y)}{\partial x}$.

For the proposed bench, we use a quadri-wave LSI (QWLSI) which diffracts then four replicas. The realization of such a LSI and its diffraction grating is amply described in Ref. 19. Notice that the QWLSI grating is an approximation of the perfect sinusoidal transmittance–the ideal grating which only diffracts four orders–, which realization would be rather complex or costly. The QWLSI allows then a full spatial characterization of a wave front, *ie* the intensity and phase measurement of the transmitted wave. Notice that this device is symmetrical with respect to polarization. In the case of the sub-wavelength gratings demonstrator, we use a QWLSI diffraction grating made of etched germanium coated with chromium.

Because of the geometry of the sample, discontinuities in the phase appear at the edge of each domain. It was shown that QWLSI can cope with discontinuous wave fronts (so-called *segmented* wave fronts since they are made by the discontinuous apposition of continuous wave fronts).[18,20] Whereas the interferogram is deformed according to the derivative of the continuous wave front, in the particular case of a segmented wave front the measure is quite different on the discontinuities: let's consider two perfect, plane wave fronts separated by a h-high step . The phase difference Δ_ϕ is then a s-wide, h-high crenel. Consequently, the interferogram is then deformed according to Δ_ϕ, which is directly proportional to the step height itself. In the case of the QWLSI the phase difference Δ_ϕ is computed along the x- and y-directions.

The transmitted intensity is determined by the analysis of the 0th-order: this is equivalent to apply a low-pass filter on the interferogram.

This solution allows then to measure both the phase shift induced by the sub-wavelength gratings and the intensity transmission, in a single measurement.

2.2 Source and detection

In the preliminary experiment we present here, we make use of a black body at $T = 1200\,^\circ\mathrm{C}$ as broad-band source. The infrared radiation is then collimated. The detection is operated by an uncooled micro-bolometer array (320×240 pixels), which detects from 8 to 12 μm. The choice of a broad-band source without spectral filtering is incompatible with a spectrally-resolved measurement, but since the AR-coating strongly absorbs

above 9 μm, one can realistically consider that the phase measurement is limited to the [8, 9 μm] spectral range. Moreover the phase variations on this spectral range are negligible (less than a few percent).

Fig. 4 illustrates the whole characterization bench. Notice that the measure was carried out with a unpolarized beam since the transverse electric (TE)-modes transmitted are highly negligible.

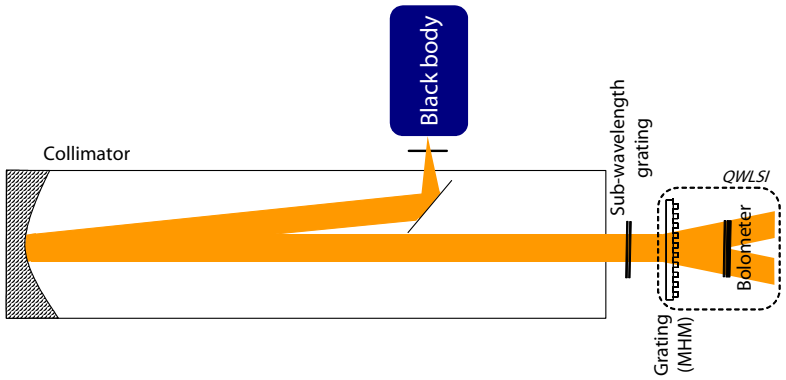

Figure 4. Experimental characterization bench dedicated to infrared sub-wavelength gratings. The QWLSI consists of a grating and the micro-bolometer.

3. EXPERIMENTAL VALIDATION

3.1 Process

Interferograms are analyzed by a Fourier Transform demodulation technique[16, 21] to extract both the derivatives of the wave front along the x- and y-direction and the transmitted intensity. Figure 5 illustrates the main steps of data extraction. A reference measurement of the wave front issued from the collimator is made; this allows to subtract the potential residual aberrations of the impinging wave front and the effects due to a possible unperfect grating.

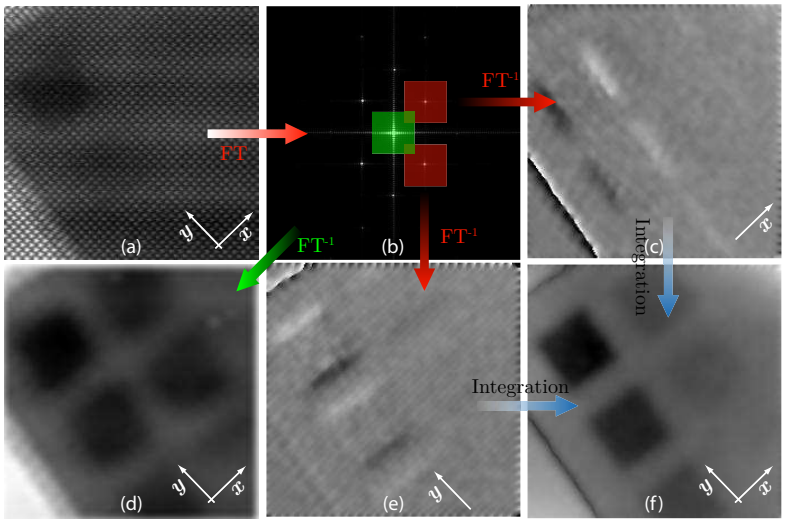

Figure 5. Data extraction from the interferogram, thanks to a Fourier analysis: the green square corresponds to the 0th-order analysis and the red squares to the harmonics analysis. The 0th-order leads to the intensity pattern of the transmitted wave whereas the harmonics lead to the derivatives of the phase.

For visualization purpose, a wave front can be reconstructed from the derivatives, using a classical iterative technique.[22, 23] Notice that the computed value of phase shift given hereafter are directly computed from the

derivatives, which contain the *purest* information of step height. Figure 6 illustrates the reconstructed phase and amplitude for each of the 6 gratings.

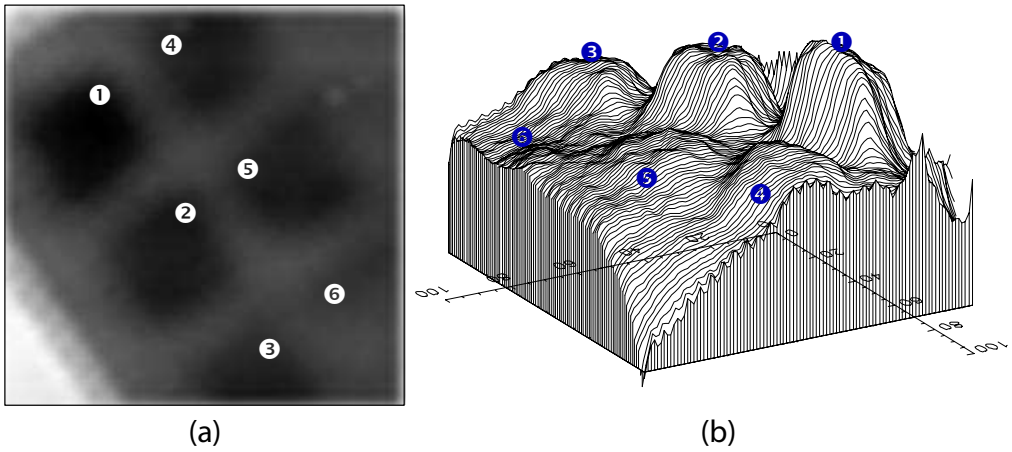

Figure 6. Reconstructed amplitude (a) and phase (b) of the demonstrator.

3.2 Transmission

The transmission of both the substrate and the sub-wavelength gratings are evaluated by QWLSI. For comparison, we carry out the same measurement using a Fourier Transform InfraRed spectrometer (FTIR). In the last case the measure is spectrally resolved and thus averaged on the detection spectral range ($[8, 9\,\mu\text{m}]$).

The measure by QWLSI is based on the microbolometer response linearity: $l = g \cdot T + o$, where l is the measured value of gray level (also called ADU or pixel count), g is the gain of the device and o an offset value. Thanks to two values of known transmission T_1 and T_2, conversion of gray levels l to transmission T is possible. We have chosen to calibrate our micro-bolometer array by matching the transmission of the first sub-wavelength grating and the bare substrate. Ideally these two references could be provided by a transparent zone and an opaque one.

Notice that the measurements by FTIR are rather different from the theoretical values given in Table 1. This is due to two major differences: first the measure by FTIR presented here is the average between the measure with a TM wave and a TE wave. Since the TE wave is almost not transmitted, the global transmission is half cut. Secondly, the calculation assumes a real index for the AR coating layers.

The results for the five gratings are summarized on Fig. 7. The error bars are evaluated by propagating the repeatability errors on the parameters g, T and o. The agreement between reference and QWLSI measurements validates the concept.

3.3 Phase

The QWLSI-measured values are summarized in Table 2. Note that the comparison is made with theoretical values calculated at $8\,\mu$m, whereas it is integrated in the spectral detection range in practice. However, as said before, the variations on the $8 - 9\,\mu$m spectral range of the phase are negligible, the comparison is then relevant.

The error bars given in Table 2 are a repeatability measurement: since the phase shift is measured around 30 times along the vertices of each square domain, a standard deviation can be calculated.

The discrepancy between the theoretical forecast and the measure for the grating ❺ is not well understood. A possible non-uniformity in the thickness of the substrate or of the AR coating may explain it. Indeed, 0.1 rad corresponds to a thickness difference of $\lambda/60$ if we consider a refractive index of $\simeq 2$ for the AR-coating, or $\lambda/100$ for a refractive index of $\simeq 3$ for the GaAs substrate.

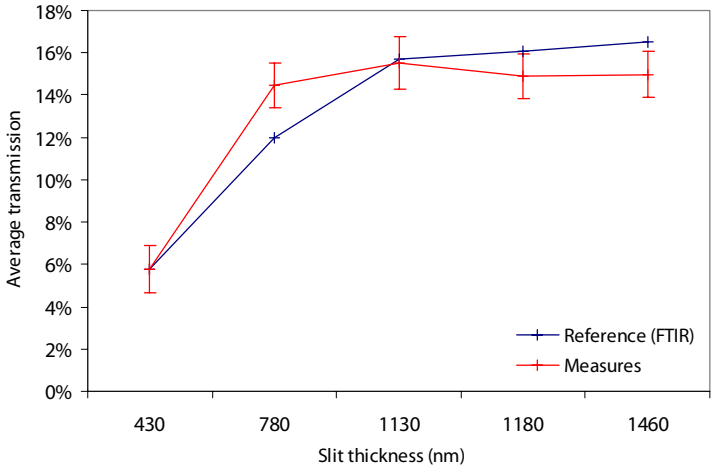

Figure 7. Comparison between the average transmissions of the five sub-wavelength gratings evaluated by QWLSI and those measured by FTIR.

Grating number	Slit thickness (nm)	Experimental phase shift (rad)	Theoretical phase shift (rad) at 8 µm
❶	430	0,92±0,08	0,88
❷	780	0,67±0,05	0,66
❸	1130	0,42±0,07	0,40
❹	1180	0,37±0,03	0,36
❺	1460	0,28±0,02	0,17

Table 2. Phase modulation induced by the sub-wavelength gratings: comparison between the expected results and the measured values.

4. CONCLUSION

We demonstrated a new technique for spatially-resolved characterizations of sub-wavelength of wide-area metallic gratings based on lateral shearing interferometry. The demonstration is based on a sample made of different sub-wavelength gratings. The proposed bench allows a full spatial characterization (*ie* phase and amplitude) of the electric field transmitted by the gratings.

The evolution of this bench to a complete spatial, spectral and directional characterization is almost straightforward. The angular resolution can be easily achieved by an *ad hoc* mechanical assembly (classical goniometric techniques). The spectral resolution is linked to a broad-band tunable source. In the infrared spectral range, one can cite parametric conversion in non-linear crystal,[24,25] super-continuum generator[26,27] used in correlation with a spectral filter or a FTIR.[28,29]

Eventually, a better efficiency in photon collection can be achieved by an improvement of the QWLSI grating: using sub-wavelength metallic gratings coding transmittances, one can realize an almost perfect sinusoidal transmittance which is the key feature of QWLSI: whereas parasitic replicas in the current QWLSI grating reduces the diffraction efficiency, a better approximation of the sinusoid would maximize the signal.[30,31]

REFERENCES

[1] Barnes, W. L., "Surface plasmon-polariton length scales: a route to sub-wavelength optics," *J. Opt. A: Pure Appl. Opt.* **8**, S87–S93 (2006).

[2] Shi, H., Wang, C., Du, C., Luo, X., Dong, X., and Gao, H., "Beam manipulating by metallic nano-slits with variant widths," *Opt. Express* **13**(18), 6815–6820 (2005).

[3] Born, M. and Wolf, E., [*Principles of Optics*], Cambridge University Press (2002).

[4] Rytov, S. M., "Electromagnetic properties of a finely stratified medium," *Sov. Phys. JETP 2* , 466–475 (1956).

[5] Vincent, G., Haïdar, R., Collin, S., Cambril, E., Velghe, S., Primot, J., Pardo, F., and Pelouard, J.-L., "Complex transmittance gratings based on subwavelength metallic structures," in [*Nanophotonics*], *Proc. SPIE* **6195** (2006).

[6] Lalanne, P., Hugonin, J., Astilean, S., Palamaru, M., and Möller, K., "One-mode model and airy-like formulae for one-dimensional metallic gratings," *J. Opt. A: Pure Appl. Opt* **2**, 48–51 (2000).

[7] Barbara, A., Quémerais, P., Bustarret, E., and Lopez-Rios, T., "Optical transmission through subwavelength metallic gratings," *Phys. Rev. B* **66**(16), 161403 (2002).

[8] Shalaev, V. M., Cai, W., Chettiar, U. K., Yuan, H.-K., Sarychev, A. K., Drachev, V. P., and Kildishev, A. V., "Negative index of refraction in optical metamaterials," *Opt. Lett.* **30**(24), 3356–3358 (2005).

[9] Dolling, G., Enkrich, C., Wegener, M., Soukoulis, C. M., and Linden, S., "Low-loss negative-index metamaterial at telecommunication wavelengths," *Opt. Lett.* **31**(12), 1800–1802 (2006).

[10] Zhang, S., Fan, W., Panoiu, N. C., Malloy, K. J., Osgood, R. M., and Brueck, S. R. J., "Experimental demonstration of near-infrared negative-index metamaterials," *Phys. Rev. Lett.* **95**(13), 137404 (2005).

[11] Klar, T., Kildishev, A., Drachev, V., and Shalaev, V., "Negative-index metamaterials: going optical," *IEEE J. Sel. Top. Quantum Electron* **12**, 1106–1115 (2006).

[12] Dolling, G., Enkrich, C., Wegener, M., Soukoulis, C., and Linden, S., "Simultaneous negative phase and group velocity of light in a metamaterial," *Science* **312**(5775), 892–894 (2006).

[13] Toulon, B., Vincent, G., Haïdar, R., Guérineau, N., Collin, S., Pelouard, J.-L., and Primot, J., "Holistic characterization of complex transmittances generated by infrared sub-wavelength gratings," *Opt. Express* **16**, 7060–7070 (2008).

[14] Malacara, D., [*Optical Shop Testing*], Wiley-Interscience, 2nd ed. (1992).

[15] Ronchi, V., "Forty years of history of a grating interferometer," *Appl. Opt.* **3**, 437–451 (1964).

[16] Primot, J., "Three-wave lateral shearing interferometer," *Appl. Opt.* **32**, 6242–6249 (1993).

[17] Primot, J. and Sogno, L., "Achromatic three-wave (or more) lateral shearing interferometer," *J. Opt. Soc. Am. A* **12**, 2679–6285 (1995).

[18] Chanteloup, J.-C., "Multiple-wave lateral shearing interferometry for wave-front sensing," *Appl. Opt.* **44**, 1559–1571 (2005).

[19] Primot, J. and Guérineau, N., "Extended hartmann test based on the pseudoguiding property of a hartmann mask completed by a phase chessboard," *Appl. Opt.* **39**, 5715–5720 (2000).

[20] Toulon, B., Primot, J., Guérineau, N., Haïdar, R., and Velghe, S., "Segmented wave-front measurements by lateral shearing interferometry," in [*Optics and Photonics*], *Proc. SPIE* **6671** (2007).

[21] Takeda, M., Ina, H., and Kobayashi, S., "Fourier-transform method of fringe-pattern analysis for computer-based topography and interferometry," *J. Opt. Soc. Am.* **72**, 156–160 (1982).

[22] Freischlad, K. R. and Koliopoulos, C. L., "Modal estimation of a wave front from difference measurements using the discrete fourier transform," *J. Opt. Soc. Am. A* **3**, 1852 (1986).

[23] Roddier, C. and Roddier, F., "Wavefront reconstruction using iterative fourier transforms," *Appl. Opt.* **30**, 1325–1327 (1991).

[24] Haïdar, R., Forget, N., Kupecek, P., and Rosencher, E., "Fresnel phase matching for three-wave mixing in isotropic semiconductors," *J. Opt. Soc. Am. B* **21**(8), 1522–1534 (2004).

[25] Ebrahim-Zadeh, M. and Sorokina, I. T., [*Mid-Infrared Coherent Sources and Applications*], ch. Mid-Infrared Optical Parametric Oscillators and Applications, 347–375 (2007).

[26] Kuo, P. S., Vodopyanov, K. L., Fejer, M. M., Simanovskii, D. M., Yu, X., Harris, J. S., Bliss, D., and Weyburne, D., "Optical parametric generation of a mid-infrared continuum in orientation-patterned gaas," *Opt. Lett.* **31**(1), 71–73 (2006).

[27] Champert, P., Couderc, V., and Barthelemy, A., "1.5-2.0-µm multiwatt continuum generation in dispersion-shifted fiber by use of high-power continuous-wave fiber source," *Photonics Technology Letters, IEEE* **16**(11), 2445–2447 (2004).

[28] Guérineau, N., Rommeluère, S., Di Mambro, E., Ribet, I., and Primot, J., "New techniques of characterisation," *Comptes rendus-Physique* **4**(10), 1175–1185 (2003).

[29] Rommeluère, S., Haïdar, R., Guérineau, N., Deschamps, J., Borniol, E. D., Million, A., Chamonal, J. P., and Destefanis, G., "Single-scan extraction of two-dimensional parameters of infrared focal plane arrays utilizing a fourier-transform spectrometer," *Appl. Opt.* **46**(9), 1379–1384 (2007).

[30] Vincent, G., Haidar, R., Collin, S., Guérineau, N., Primot, J., Cambril, E., and Pelouard, J.-L., "Realization of sinusoidal transmittance with subwavelength metallic structures," *J. Opt. Soc. Am. B* **25**(5), 834–840 (2008).

[31] Haïdar, R., Toulon, B., Vincent, G., Collin, S., Velghe, S., Primot, J., and Pelouard, J.-L., "Optical wavefront sensor based on sub-wavelength metallic structures," in [*Optics and Photonics*], *Proc. SPIE* (2008).